Cell Reports
Article

Tricarboxylic Acid Cycle Activity and Remodeling of Glycerophosphocholine Lipids Support Cytokine Induction in Response to Fungal Patterns

Saioa Márquez,[1,7] José Javier Fernández,[1,7] Cristina Mancebo,[1] Carmen Herrero-Sánchez,[1,2] Sara Alonso,[2] Tito A. Sandoval,[3,4,5] Macarena Rodríguez Prados,[1,2] Juan R. Cubillos-Ruiz,[3,4,5] Olimpio Montero,[6] Nieves Fernández,[1,2] and Mariano Sánchez Crespo[2,8,*]

[1]Departamento de Bioquímica y Biología Molecular, Facultad de Medicina, Universidad de Valladolid, 47005 Valladolid, Spain
[2]Instituto de Biología y Genética Molecular, CSIC-Universidad de Valladolid, 47003 Valladolid, Spain
[3]Weill Cornell Graduate School of Medical Sciences, Cornell University, New York, NY 10065, USA
[4]Department of Obstetrics and Gynecology, Weill Cornell Medicine, New York, NY 10065, USA
[5]Sandra and Edward Meyer Cancer Center, Weill Cornell Medicine, New York, NY 10065, USA
[6]Centro para el Desarrollo de la Biotecnología, CSIC, Parque Tecnológico de Boecillo, 47151 Valladolid, Spain
[7]These authors contributed equally
[8]Lead Contact
*Correspondence: mscres@ibgm.uva.es
https://doi.org/10.1016/j.celrep.2019.03.033

SUMMARY

Increased glycolysis parallels immune cell activation, but the role of pyruvate remains largely unexplored. We found that stimulation of dendritic cells with the fungal surrogate zymosan causes decreases of pyruvate, citrate, itaconate, and α-ketoglutarate, while increasing oxaloacetate, succinate, lactate, oxygen consumption, and pyruvate dehydrogenase activity. Expression of *IL10* and *IL23A* (the gene encoding the p19 chain of IL-23) depended on pyruvate dehydrogenase activity. Mechanistically, pyruvate reinforced histone H3 acetylation, and acetate rescued the effect of mitochondrial pyruvate carrier inhibition, most likely because it is a substrate of the acetyl-CoA producing enzyme ACSS2. Mice lacking the receptor of the lipid mediator platelet-activating factor (PAF; 1-*O*-hexadecyl-2-acetyl-*sn*-glycero-3-phosphocholine) showed reduced production of IL-10 and IL-23 that is explained by the requirement of acetyl-CoA for PAF biosynthesis and its ensuing autocrine function. Acetyl-CoA therefore intertwines fatty acid remodeling of glycerophospholipids and energetic metabolism during cytokine induction.

INTRODUCTION

Mononuclear phagocytes show high plasticity and undergo metabolic and transcriptional rewiring to cope with the challenges posed by pathogen-associated molecular pattern (PAMP) processing and the production of inflammatory mediators. The association of the inflammatory response with increased glycolysis, a process termed aerobic glycolysis or the Warburg effect, has been related to the generation of metabolic precursors for anabolic processes (Krawczyk et al., 2010). In many cases, these changes are paralleled by a drop of oxidative phosphorylation (OXPHOS), but recent studies showed that increased glycolysis may coincide with stable oxygen consumption rate (OCR) and pyruvate flux (Meiser et al., 2016; Márquez et al., 2017). The conversion of pyruvate into acetyl-CoA by the pyruvate dehydrogenase complex (PDC) is critical for the expression of *Nos2*, *Irg1*, and *Tnf* in murine macrophages stimulated with lipopolysaccharide (LPS) (Meiser et al., 2016). Pyruvate flux has also been related to the induction of IL-1β, IL-6, and PD-L1 (Shirai et al., 2016; Watanabe et al., 2017). These findings highlight the role of the tricarboxylic acid (TCA) cycle and bring into prominence the functions of pyruvate kinase (PK) M2, the enzyme that catalyzes the last step of glycolysis and also has protein kinase activity (Gao et al., 2012).

There are two breaks in the TCA cycle in macrophages—after citrate (Jha et al., 2015) and after succinate (Tannahill et al., 2013)—as well as anaplerotic compensations. Citrate influences cytokine induction (MacPherson et al., 2017), inhibits PDC (Taylor and Halperin, 1973) and yields acetyl-CoA in the cytoplasm-nucleus compartment after its conversion by ATP citrate lyase (ACLY) into oxaloacetate and acetyl-CoA. Citrate is also a precursor for itaconate synthesis via *cis*-aconitate decarboxylase (Michelucci et al., 2013). Acetyl-CoA is a carbon-source rheostat, the production of which is maintained under conditions of limited supply of glucose and oxygen. Acetyl-CoA can be yielded by fatty acid oxidation (Vats et al., 2006), reductive carboxylation of glutamine, transamination of branched-chain amino acids (Papathanassiu et al., 2017), and the ligation of acetate to CoA by acyl-CoA synthetase short-chain family 2 (ACSS2) because acetate is an abundant circulating carbon metabolite (Hui et al., 2017). Under glucose deprivation, ACSS2 translocates to the nucleus to produce acetyl-CoA for histone acetylation (Li et al., 2017; Mews et al., 2017), while cytoplasmic ACSS2 supports lipogenesis (Comerford et al., 2014) and most likely lipid mediator biosynthesis. In fact, acetyl-CoA serves as a substrate for the formation of arachidonate (AA) via linoleic acid elongation (Salem et al., 1999) and the biosynthesis of platelet-activating factor (PAF; 1-*O*-hexadecyl-2-acetyl-*sn*-glycero-3-phosphocholine). This biosynthesis involves two enzymatic

steps: (1) the hydrolysis of 1-*O*-hexadecyl-2-arachidonyl-*sn*-3-glycerophosphocholine by the cytosolic phospholipase A_2 ($cPLA_2$) (Uozumi et al., 1997) and (2) the acetylation of the resulting lyso-phospholipid moiety (lyso-PAF) by the Lands' cycle enzyme lysophosphatidylcholine acyltransferase (LPCAT) 2 (Morimoto et al., 2014). These data are of pathophysiological relevance because PAF displays many proinflammatory effects. Mice with deletion of PAF receptor (Ptafr) show a marked reduction of systemic anaphylaxis and a normal response to bacterial endotoxin (LPS) (Ishii et al., 1997). Conversely, transgenic mice hyperexpressing Ptafr are hypersensitive to LPS (Ishii et al., 1998). Notably, patients with low levels of the enzyme PAF acetylhydrolase show an increased risk for lethal anaphylaxis (Vadas et al., 2008). Recently, the list of PAF effects has been enlarged by the report of its involvement in a feedforward autocrine signaling mechanism that enhances the production of IL-10 (Koga et al., 2013, 2017) and IL-23 (Rodríguez et al., 2016).

In this study, we analyzed the role of intermediary metabolites in the production of cytokines by monocyte-derived dendritic cells (DCs), focusing on IL-10 and IL-23 in view of the available information on their modulation by lipid mediators. Experiments showed (1) a critical dependence on pyruvate flux of the acetylation of histone H3 in the *IL10* and *IL23A* promoters, (2) a route of acetyl-CoA production via ACSS2 that rescues the blockade of the mitochondrial pyruvate carrier, and (3) further evidence of the autocrine role of PAF in the production of IL-10 and IL-23 using *Ptafr*$^{-/-}$ mice. In summary, we uncovered a regulatory mechanism of cytokine induction that involves acetylation of histones and signaling through the Ptafr. This mechanism links fatty acid-glycerophospholipid remodeling with energetic metabolism via acetyl-CoA.

RESULTS

Pyruvate and Acetate Modulate Cytokine Production

A recent study combining pharmacological inhibition of pyruvate flux and stable isotope-assisted metabolomics techniques disclosed the dependence of *Tnf* induction on pyruvate oxidation, while *Il1b* gene expression was not significantly inhibited, thus pointing to specificity in the control of cytokine expression by mitochondrial activity (Meiser et al., 2016). On the basis of this report and our previous study showing that increased glycolysis was coincidental with the maintenance of the OCR, the effect of the pyruvate mitochondrial carrier inhibitor UK5099 was assessed (Figure S1A). UK5099 inhibited the expression of *IL23A*, *IL1B*, *TNF*, and *IL10* mRNA to a different extent. Maximal effects were observed in the case of *IL23A* and *IL10* in zymosan-stimulated DCs (Figure 1A). Conversely, enhancing PDC activity through the inhibition of its physiological negative regulator pyruvate dehydrogenase kinase by dichloroacetate (DCA) increased *IL23A* and *IL10* mRNA expression (Figure 1B). The activity of the PDC was assessed by assaying the inhibitory phosphorylation of S293-PDH E1-α subunit. Resting DCs showed this phosphorylation to a high extent, which was decreased by zymosan stimulation and increased by citrate (Figure 1C). The addition of acetate to feed the production of acetyl-CoA via ACCS2 increased the production of both *IL23A* and *IL10* mRNA and partially countered the effect of UK5099 (Figure 1A). To scrutinize the mechanism that associates cytokine expression with pyruvate flux and likely with NADH turnover, the effect of UK5099 on the bioenergetic profile and the effect of inhibiting complex I activity with rotenone were assessed. UK5099 blocked the increase of the OCR and the extracellular acidification rate (ECAR) induced by zymosan (Figure 1D). Rotenone partially mimicked the effect of UK5099 because it inhibited *IL10* and *IL23A* mRNA expression, while its effect on *TNF* and *IL1B* mRNA was inconsistent (Figure 1E). These results suggest that pyruvate may reinforce *IL23A* and *IL10* transcription by maintaining electron transport chain activity at complex I.

The assay of intermediary metabolites showed a rewiring coincidental with the time course of phagocytic uptake (Valera et al., 2008), the dephosphorylation of S293-PDH E1-α subunit, and the bioenergetic profile. Zymosan strongly reduced pyruvate and increased lactate, thus making the lactate/pyruvate ratio reach values similar to those reported in muscle (Brooks, 2018), in which the minimal lactate/pyruvate ratio is 10 and increases above 100 when glycolysis increases. Zymosan caused a drop of citrate, itaconate, and the α-ketoglutarate/succinate ratio, while oxaloacetate levels increased and malate did not show any significant change (Figure 2). Acetate partially countered the effect of zymosan on the lactate/pyruvate ratio (Figure 2A) and decreased oxaloacetate levels (Figure 2D). In addition, acetate partially rescued the drops of citrate and α-ketoglutarate and increased acetyl-CoA levels (Figures 2B and 2C).

Because zymosan's effects depend on signals conveyed at least by dectins and Toll-like receptors (TLRs), experiments were conducted with depleted zymosan, a derivative of zymosan that lacks the mannose fraction involved in dectin-2 and TLR signaling (Gantner et al., 2003). Depleted zymosan induced a reduced phagocytic cargo (Figure 2E) and less than 25% of the cytokine induction elicited by zymosan (Figure 2F). The metabolic profile was different from that induced by zymosan, because the levels of pyruvate and citrate and the α-ketoglutarate/succinate ratio were not reduced (Figure 2G). These results indicate that both cytokine induction and metabolic rewiring are strongly dependent on the combined activation of different receptors.

The metabolic program induced by LPS showed increases of lactate and itaconate, the absence of citrate drop, and a stable α-ketoglutarate/succinate ratio (Figures S1B–S1E). A plausible reason for the limited response of DCs to LPS compared with zymosan might be the reduction of CD14 expression associated with the differentiation process (Figure S1F). Together, these data indicate an intensive consumption-rerouting of pyruvate in the initial steps of phagocytosis, a partial rescue of the depletion of some intermediates by acetate, and a strong dependence of the expression of *IL23A* and *IL10* on pyruvate supply.

PKM2 Activity and Cytokine Induction

DCs showed a high amount of PKM2 tetramers, the level of which was not increased by PAMPs or by ML-265/TEPP-46, an activator of its assembly and glycolytic activity (Anastasiou et al., 2012) (Figure S2A). ML-265 did not influence extracellular lactate levels or the response to LPS. In contrast, it reduced *TNF*, *IL10*, *IL23A*, *IL1B*, and *PDL1* mRNA expression in response to zymosan (Figure S2B). Given that Y705-STAT3 and S10-histone

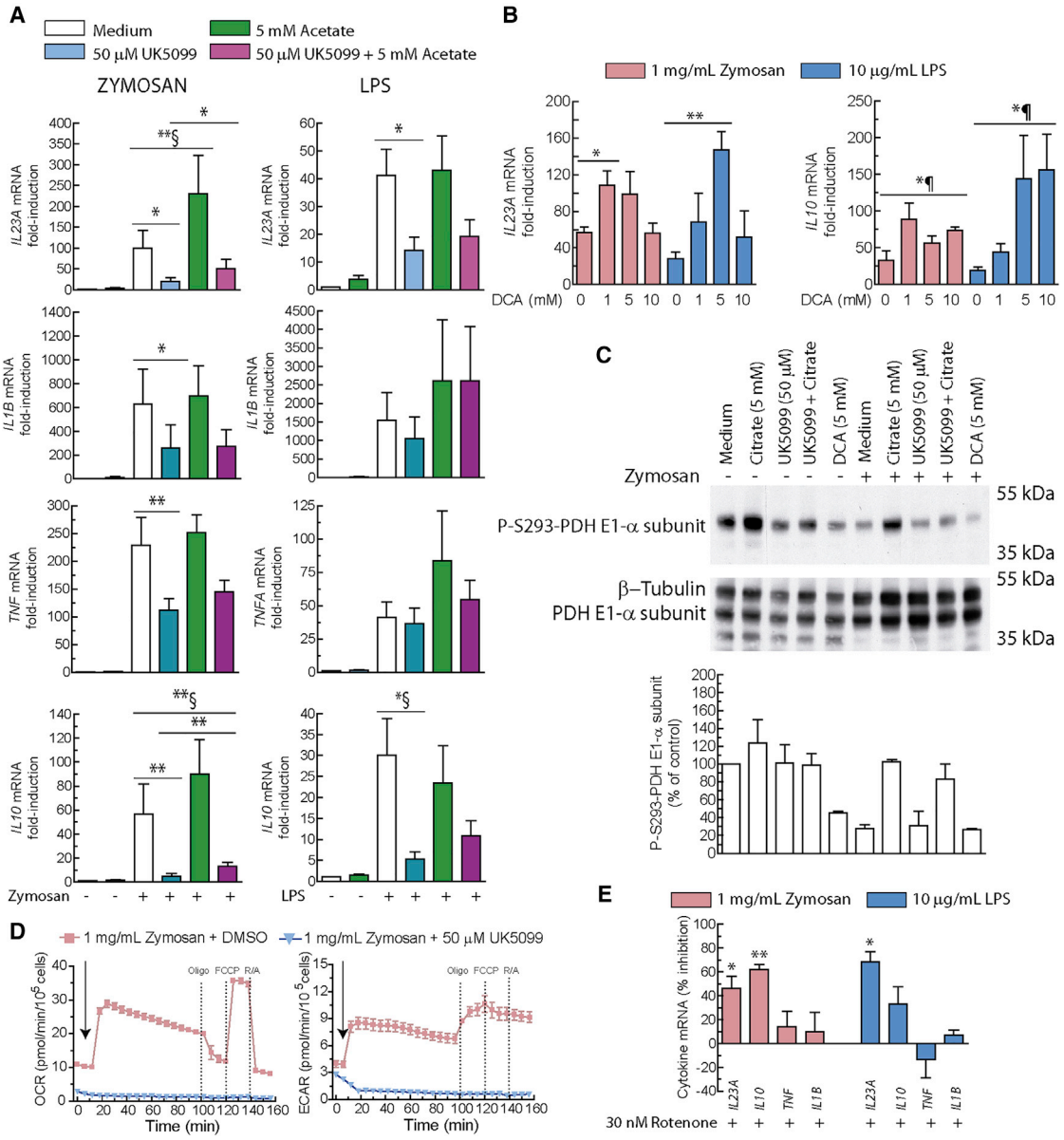

Figure 1. Effect of the Inhibition of the Mitochondrial Pyruvate Carrier and of Acetate Supplementation on the Expression of the mRNA of Several Cytokines

(A) DCs were preincubated with the indicated additions for 1 h prior to stimulation with 1 mg/mL zymosan and 10 μg/mL LPS. After 4 h of incubation, the RNA was extracted and used for the assay of the mRNA encoding the cytokines. Data are presented as mean ± SEM (n = 4–14). *p < 0.05 and **p < 0.01, two-tailed Student's t test; §Wilcoxon signed-rank test.

(B) Effect of the inhibition of pyruvate dehydrogenase kinase with DCA. Mean ± SEM (n = 3). *p < 0.05 and **p < 0.01, two-tailed Student's t test; Friedman test.

(C) Phosphorylation of P-S293-PDH E1-α subunit in DCs treated with 5 mM citrate, 50 μM UK5099, or 5 mM DCA for 1 h and then stimulated with zymosan for 30 min. The membrane was blotted with anti-P-S293-PDH E1-α antibody (Ab) and then stripped and sequentially reblotted with anti-PDH E1-α Ab and anti-β-tubulin Ab. The densitometric analysis represents two independent experiments.

(D) Recordings of the XF Mito Stress Test protocol obtained in DCs stimulated with zymosan in the presence and absence of 50 μM UK5099. DCs were stimulated with zymosan (arrows) and the changes of OCR and ECAR recorded. Dotted lines indicate the time of injection of the components of the Mito Stress Test Kit (1 μM oligomycin, 1.5 μM FCCP, and 100 nM rotenone plus 1 μM antimycin).

(E) Effect of the inhibition of the electron transport chain by incubation for 30 min with 30 nM rotenone on the mRNA expression of cytokines in DCs treated with zymosan or LPS for 4 h. Mean ± SEM (n = 3). *p < 0.05 and **p < 0.01, two-tailed Student's t test.

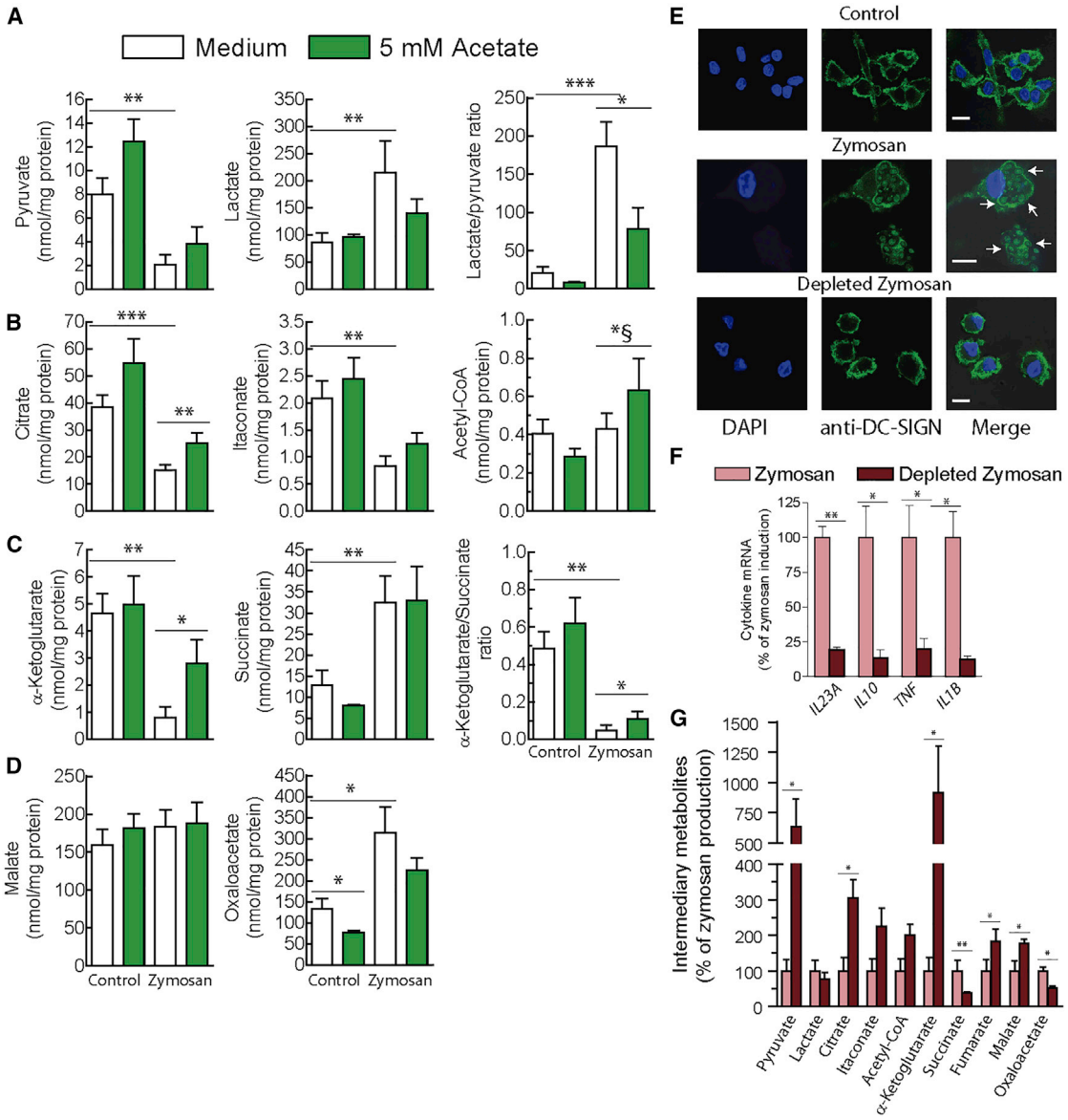

Figure 2. Assay of TCA Cycle Intermediates and Effect of Exogenous Acetate

(A–D) DCs were preincubated in the presence and absence of acetate for 1 h prior to stimulation with 1 mg/mL zymosan particles, and 30 min thereafter, metabolites were extracted for the ultraperformance liquid chromatography and mass spectrometry (UPLC/MS) analysis of pyruvate and lactate (A), citrate, itaconate, and acetyl-CoA (B), α-ketoglutarate and succinate (C), and malate and oxaloacetate (D). Results represent mean ± SEM (n = 4–14). *p < 0.05, **p < 0.01, and ***p < 0.001, two-tailed Student's t test; §Wilcoxon signed-rank test.

(E) DCs take up zymosan particles. DCs adhered to poly-ornithine coated plates were incubated with zymosan particles for 1 h. At the end of this period, DCs were fixed and stained with anti-DC-SIGN Ab. DCs show a larger cytoplasm an engulfed zymosan particles (arrows), while these were scarcely observed in DCs treated with depleted zymosan.

(F and G) Comparison of the effect of 1 mg/mL zymosan and 1 mg/mL depleted zymosan on the induction of cytokine mRNA expression (F) and intracellular metabolite levels (G). Scale bar represents 10 μm. Results are expressed as percentage of the response induced by zymosan and represent mean ± SEM (n = 4). *p < 0.05 and **p < 0.01, Student's t test.

See also Figures S1–S3.

H3 are among the best characterized protein substrates phosphorylated by the monomeric-dimeric form of PKM2, the effect of ML-265 was interrogated. ML-265 inhibited the phosphorylation of STAT3 (Figure S2C). In contrast, a definite inhibition of S10-histone H3 phosphorylation and of K9- and K14-histone H3 acetylation was not observed (Figures S2D and S2E). The assay of metabolic intermediates showed a trend to decrease the levels of pyruvate in resting cells, and a reduction of α-ketoglutarate upon LPS treatment, but a definite metabolic rewiring could not be established (Figure S1). A further attempt to

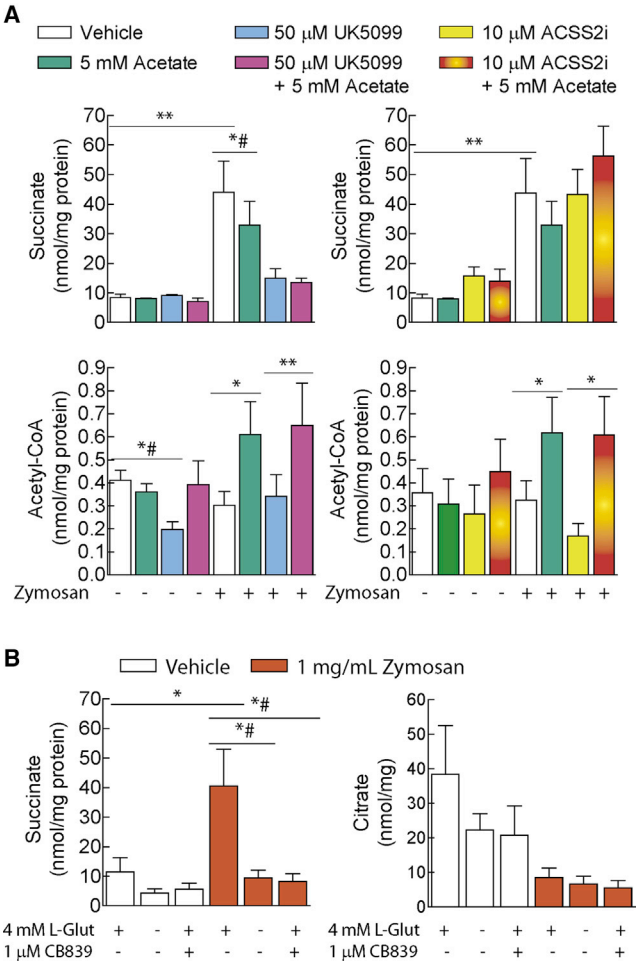

Figure 3. Effect of the Inhibition of the Mitochondrial Pyruvate Carrier and ACSS2 and Glutaminase Activities on Succinate and Acetyl-CoA Levels

(A) DCs were preincubated with the indicated additions for 1 h. At the end of this period, DCs were stimulated with 1 mg/mL zymosan for 30 min, and cell lysates collected for the assay. Mean ± SEM (n = 3–7). *p < 0.05 and **p < 0.01, two-tailed Student's t test; #Mann-Whitney test.

(B) Effect of glutamine depletion on succinate and citrate levels. DCs were starved of glutamine (L-Glut) for 1 h or incubated for 30 min in the presence of the glutaminase inhibitor CB839. At the end of this period, zymosan or vehicle was added for an additional period of 30 min, and cell lysates were collected. Mean ± SEM (n = 4–11). *p < 0.05 and **p < 0.01, two-tailed Student's t test; #Mann-Whitney test.

See also Figure S4.

decipher the effect of ML-265 was carried out using real-time bioenergetic monitoring. As shown in Figure S3, 50 μM ML-265 did not influence the bioenergetic profile. Of note, LPS did not influence the OCR and slightly enhanced the ECAR, while zymosan steadily enhanced both the OCR and the ECAR for ~50 min, followed by a period of stabilization and maintenance of the spare respiratory capacity for at least 120 min. The concentrations of lactate in the extracellular medium after stimulation for 24 h by zymosan and LPS were similar (Figure S2B), while intracellular lactate was lower in LPS-treated DCs at 30 min (Figure S1A). This can be explained by the distinct mechanisms whereby PAMPs enhance glycolysis. The effect of zymosan is reminiscent of the early translocation of hexokinase II to the mitochondrial membrane reported by Everts et al., (2014), who observed that HIF1α-dependent induction of glycolytic enzymes is not involved in the rapid changes in glycolytic metabolism observed in murine DCs stimulated by TLR agonists. Because the assembly of PKM2 and lactate production were not influenced by ML-265, the effect on cytokine induction could be explained by interference with the protein kinase activity of PKM2 on substrates other than those assayed in the present experiments. Alternatively, an off-target effect of ML-265 cannot be ruled out.

The Role of Succinate

The high levels of succinate detected and its reported role in the inflammatory response through HIF1α stabilization (Palsson-McDermott et al., 2015) and the SUCN1/GPR91 receptor (Rubic et al., 2008) prompted us to address the expression and function of SUCN1. About 10% of the DCs showed a detectable expression of SUCNR1 by immunofluorescence flow cytometry (Figure S4A). This was confirmed in immunofluorescence confocal microscopy studies in which only a fraction of DCs showed positive staining (Figure S4B). Treatment with zymosan and LPS for 4 h induced a marked reduction of *SUCNR1* mRNA expression (Figure S4C). In keeping with this reduction, zymosan-treated DCs did not show Ca^{2+} transients in response to both succinate and fumarate, while they responded to a purinergic agonist, therefore ruling out a general inhibition of G protein-coupled receptor (GPCR) function (Figure S4D). Exogenous succinate did not influence *IL23A* and *IL10* mRNA expression or the release of AA metabolites (Figures S4E and S4F). Because succinate can be produced from pyruvate and anaplerotic glutamine, pyruvate flux and glutaminase activity were inhibited. Acetate did not rescue the drop of succinate levels induced by UK5099, although it surmounted the effect of both UK5099 and an inhibitor of ACSS2 (ACSS2i) on acetyl-CoA levels (Figure 3A). Inhibition of glutaminase activity by 1 μM CB839 decreased the levels of succinate to a similar extent to those induced by glutamine starving (Figure 3B). Unexpectedly, the decrease of succinate levels induced by these treatments did not correlate with cytokine induction, as CB839 only showed inhibitory effects at concentrations of 5–10 μM (i.e., significantly higher than those decreasing succinate levels), which suggests an off-target effect. These data indicate that the effect of succinate is best explained via interaction with an intracellular target(s) and/or changes in the α-ketoglutarate/succinate ratio, in keeping with the notion that a low ratio is associated with Jumonji domain-containing demethylase 3-dependent enhancement of the proinflammatory phenotype in macrophages (Liu et al., 2017).

Roles of ACLY and ACSS2

DCs have significant expression of *ACLY* and *ACSS2* mRNA. Unlike *PDL1*, the expression of the mRNA of those enzymes decreased after zymosan treatment, which suggests a high transcription rate under resting conditions (Figure 4A). The ACLY inhibitor BMS 303141 decreased the induction of *IL1B*

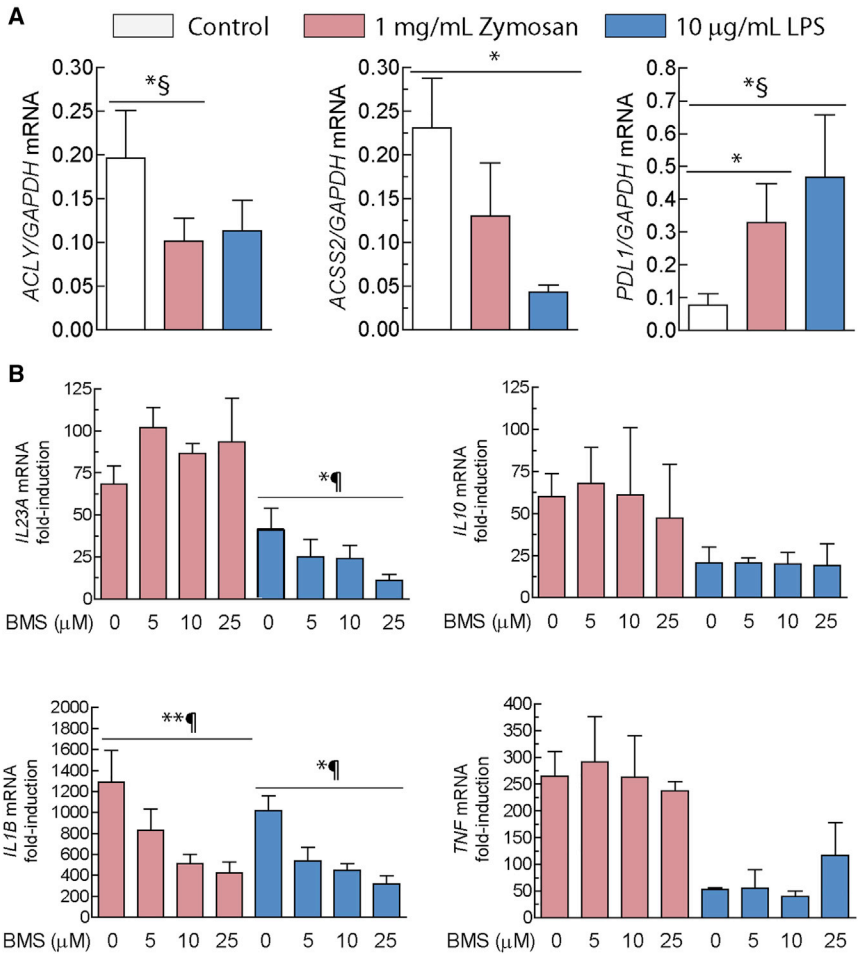

Figure 4. Expression of *ACLY*, *ACSS2*, and *PDL1* mRNA

(A) DCs were incubated in the presence and absence of zymosan or LPS for 4 h. At the end of this period, RNA was collected for the assay of the indicated transcripts. Mean ± SEM (n = 7). *p < 0.05, two-tailed Student's t test; §Wilcoxon signed-rank test.

(B) DCs were preincubated with different concentrations of the ACLY inhibitor BMS 303141 for 1 h, and after 4 h of stimulation, the RNA was collected to assay the expression of the mRNA of the cytokines. Mean ± SEM (n = 3). *p < 0.05 and **p < 0.01; Friedman test.

induced by both zymosan and LPS and the induction of *IL23A* in response to LPS (Figure 4B). ACSS2i showed a trend to inhibit the induction of *IL23A* mRNA elicited by zymosan, while robustly inhibiting the effect of exogenous acetate. In contrast, the effect of LPS was not influenced by ACSS2i (Figure 5A, top). ACSS2i decreased the effect of acetate on the *IL10* mRNA expression induced by zymosan, while inhibiting the effect of LPS only in the absence of acetate (Figure 5A, bottom). ACSS2i also decreased the enhanced expression of *IL23A* observed in the presence of 2-deoxyglucose (2-DG) (Figure 5B), a glycolytic inhibitor that, similar to hypoxia and glucose starving, enhances ACSS2 activity (Bulusu et al., 2017; Li et al., 2017) and *IL23A* expression (Márquez et al., 2017). ACSS2 protein showed a predominant cytoplasmic expression, the distribution of which between nuclear and cytoplasmic compartments was not significantly influenced by UK5099 and acetate (Figure 5C). 2-DG only slightly increased the amount of nuclear ACSS2 (Figure 5D). Because acetate rescues the effect of both UK5099 and ACSS2i on acetyl-CoA levels (Figure 3A), these results suggest that under conditions of low formation of acetyl-CoA from pyruvate, ACSS2 may replenish the cytoplasmic-nuclear pool and support cytokine transcription.

Histone H3 Acetylation of *IL23A* and *IL10* Promoters

The acetylation of K9-histone H3 was interrogated in view of its role on the opening of the chromatin structure. Zymosan and LPS increased the acetylation of the proximal κB-site of the *IL23A* promoter, while UK5099 showed an inhibitory effect. Acetate did not increase the effect of zymosan and showed a trend to inhibit the effect of LPS (Figure 6A). Consistent with the involvement of CRE-dependent *trans*-activation of *IL10* by zymosan, an increase of K9-histone H3 acetylation sensitive to UK5099 was observed (Figure 6A). BMS 303141 did not elicit any significant effect on histone H3 acetylation at both κB and CRE sites, while DCA showed a significant increase (Figure 6B). To address whether the acetylation of the promoters correlated with global changes of histone acetylation, P-S10 and acetyl-K9-histone H3 were assayed in cell lysates (Figure 6C). Experiments disclosed an increase of S10-histone H3 phosphorylation and acetylation in the case of zymosan, together with a slight delay of migration, most likely dependent on post-translational modifications. These results suggest that pyruvate supply influences histone H3 acetylation at the *IL23A* and *IL10* promoters and that these changes correlate with cytokine expression induction better than the overall changes in K9-histone H3 acetylation.

Cytokine Production by WT and *Ptafr*$^{-/-}$ Mice

Given the role of acetyl-CoA in PAF biosynthesis (Figure S5) and the autocrine function of PAF in the production of cytokines, we set out experiments in bone marrow-derived DCs (BMDCs) from mice with genetic deletion of the Ptafr. Wild-type (WT) mice showed a higher production of IL-23 protein than *Ptafr*$^{-/-}$ mice (Figure 7A, left sets of data). In contrast, there was no difference in the response to LPS (Figure 7B). UK5099 inhibited IL-23 production in WT mice in response to zymosan to an extent similar to that observed in human DCs. Acetate supplementation increased the production in WT mice and countered the effect of UK5099. In contrast, the enhancing effect of acetate was

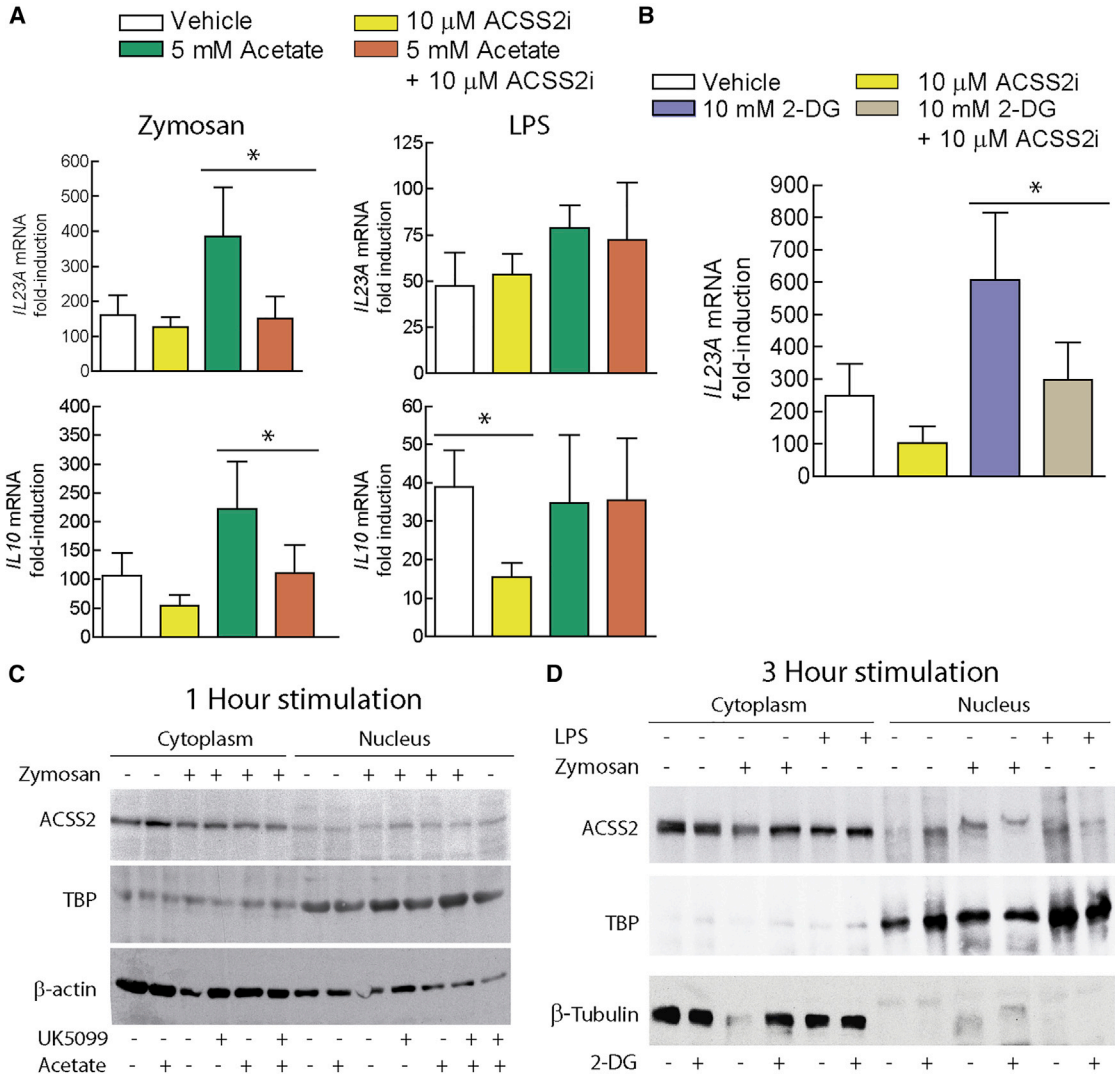

Figure 5. Effect of ACSS2i on the Expression of *IL23A* and *IL10* mRNA

(A) DCs were incubated in the presence and absence of exogenous acetate for 1 h. RNA extraction was carried out after 4 h of stimulation with 1 mg/mL zymosan or 10 μg/mL LPS. Mean ± SEM (n = 4–8). *p < 0.05, two-tailed Student's t test.

(B) Effect of 10 μM ACSS2i on the enhancement of *IL23A* mRNA expression induced by preincubation with 10 mM 2-DG 1 h prior to the stimulation by zymosan. RNA was collected after 4 h of stimulation. Mean ± SEM (n = 5). *p < 0.05, two-tailed Student's t test.

(C) Expression of ACSS2 protein in cytoplasmic and nuclear fractions of DCs after 1 h of stimulation in the presence of 50 μM UK5099 and 5 mM acetate.

(D) Effect of 10 mM 2-DG on the expression of ACSS2 protein in the cytoplasmic and nuclear fractions after 3 h of stimulation.

not observed in the *Ptafr*$^{-/-}$ mice (Figures 7A and 7B). The production of IL-10 by *Ptafr*$^{-/-}$ mice was significantly lower than that observed in WT mice, and the effect of UK5099 was not countered by acetate (Figures 7C and 7D). Consistent with the results obtained in the assay of proteins, *Ptafr*$^{-/-}$ mice showed a reduced induction of the mRNA of *Il23a* in response to zymosan (Figure 7E).

The phosphorylation of Y705-STAT3 was addressed because STAT3 has been associated with the transcriptional regulation of *Il10*. However, no differences were observed between WT and *Ptafr*$^{-/-}$ mice (Figure 7F). Together, these results indicate that a fraction of the role played by pyruvate in the production of IL-10 and IL-23 may be associated with the autocrine production of PAF, consistent with the involvement of acetyl-CoA in its biosynthesis. Although IL-23 production showed an acetate- and PAF-dependent step in response to zymosan, the results on IL-10 production, although clearly dependent on the Ptafr, were not enhanced by acetate, thus suggesting that PAF may exert effects at a concentration reached without fueling acetyl-CoA production with supplemental acetate.

DISCUSSION

These results shed light on the role of energetic metabolism in cytokine induction by showing that the mRNA expression of *IL23A*, *IL10*, *IL1B*, and *TNF* depends on the activity of the

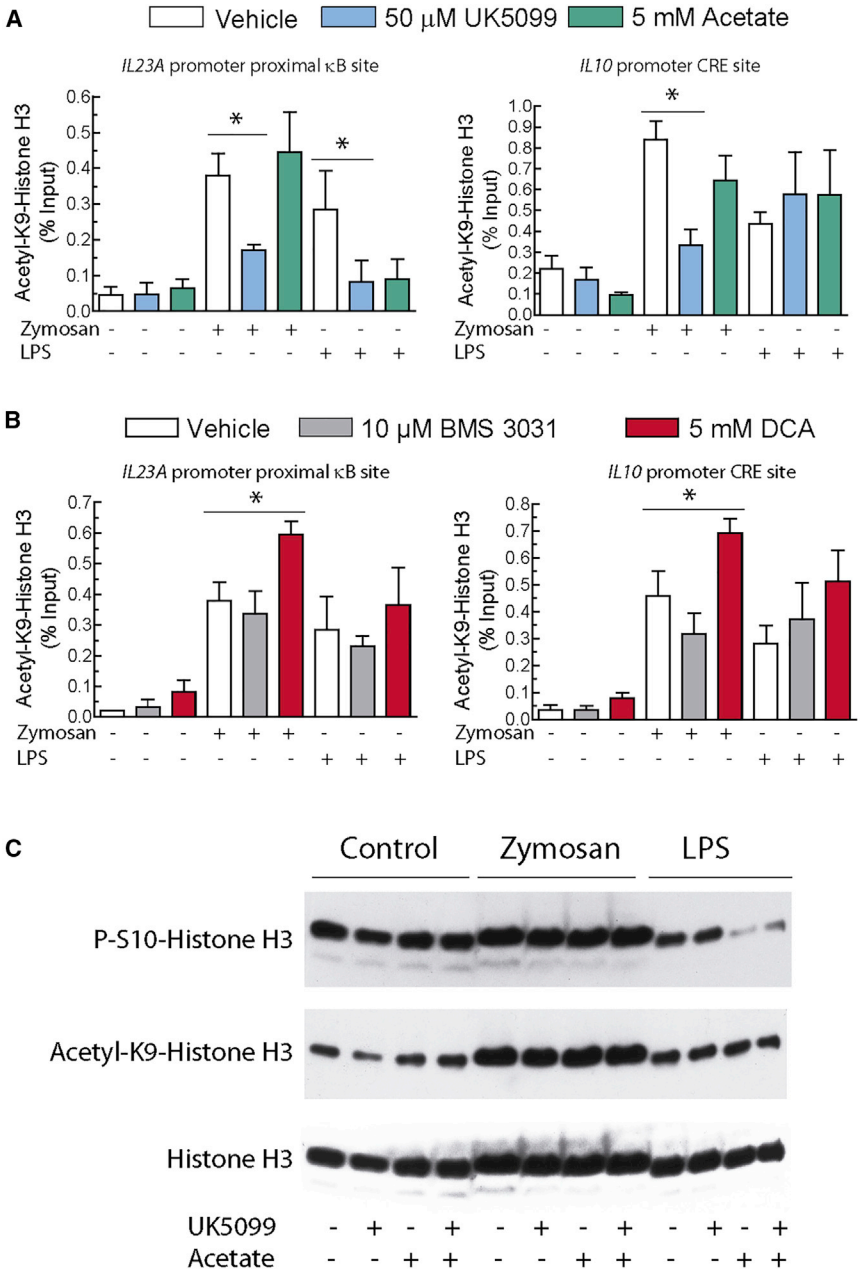

Figure 6. Effect of Different Treatments on the Acetylation of K9-Histone H3 in the Areas Flanking the Proximal κB-site of the *IL23A* Promoter and the CRE Site of *IL10* Promoter

(A) DCs were preincubated in the presence and absence of UK5099 and acetate for 1 hour and then stimulated with 1 mg/mL zymosan particles or 10 μg/mL LPS for 30 min. At the end of this period, cell lysates were collected for chromatin immunoprecipitation (ChIP) assays to address the acetylation of *IL23A* and *IL10* promoters. Mean ± SEM (n = 3). *p < 0.05, two-tailed Student's t test.

(B) Effect of BMS 303141 and DCA on promoter acetylation. Mean ± SEM (n = 4 or 5).

(C) Effect of UK5099 and acetate on global S10-histone H3 phosphorylation and K9-histone H3 acetylation. Incubation periods and concentration of stimuli are as in (A).

pyruvate mitochondrial carrier. The activity of PDC under zymosan stimulation was warranted by the low values of OCR and ECAR in the presence of UK5099 and the decrease of P-S293-PDH E1-α subunit, which suggests that the increase of enzyme activity may explain the reduced level of pyruvate and agrees with reports in LPS-stimulated macrophages, in which PDH activity was maintained by a repression of PDH kinase 1 and a low level of P-S293-PDH E1-α (Meiser et al., 2016). The effect of UK5099 was strongest on *IL23A* and *IL10* mRNA expression and countered by acetate at concentrations similar to those detected in serum after bacterial infection (Balmer et al., 2016). Because acetate drives the production of acetyl-CoA, a cogent explanation could be that the entry of pyruvate into the TCA cycle feeds the formation of cytoplasmic acetyl-CoA via the citrate shuttle and ACLY activity. Recent evidence on the role of pyruvate import was provided using ML-265 (Shirai et al., 2016; Watanabe et al., 2017). However, ascertaining the overall effect of ML-265 is a difficult task, given the complex metabolic scenario it sets out. A mechanistic explanation may be its ability to render PKM2 tetramers resistant to dissociation by phosphotyrosine-containing proteins (Anastasiou et al., 2012) (i.e., a signaling mechanism widely used by C-type lectin receptors). Because experiments did not disclose changes in lactate production, a possible explanation can be that the partition of PKM2 between monomer-dimer and tetramer assemblies is cell specific. Given that a metabolic profile associated with ML-265 could not be depicted and the phosphorylation of STAT3 at Y705 was inhibited, it seems likely that the effect of PKM2 on cytokine production might depend on its protein kinase activity.

The low levels of itaconate induced by zymosan can be explained by the low citrate levels. This differs from the increase observed in response to LPS and agrees with the findings of Domínguez-Andrés et al. (2019), who reported that although LPS is a robust inducer of the *cis*-aconitate decarboxylase encoded by *IRG1*, β-glucans do not induce the enzyme and even block the effect of LPS. Itaconate has been functionally associated with the cytokine signature via the electron transport chain (Lampropoulou et al., 2016) and the alkylation of KEAP1 (Mills et al., 2018). Overall, the combination of a low α-ketoglutarate/succinate ratio and a low level of itaconate helps explain the robust proinflammatory effects of zymosan. Additional features

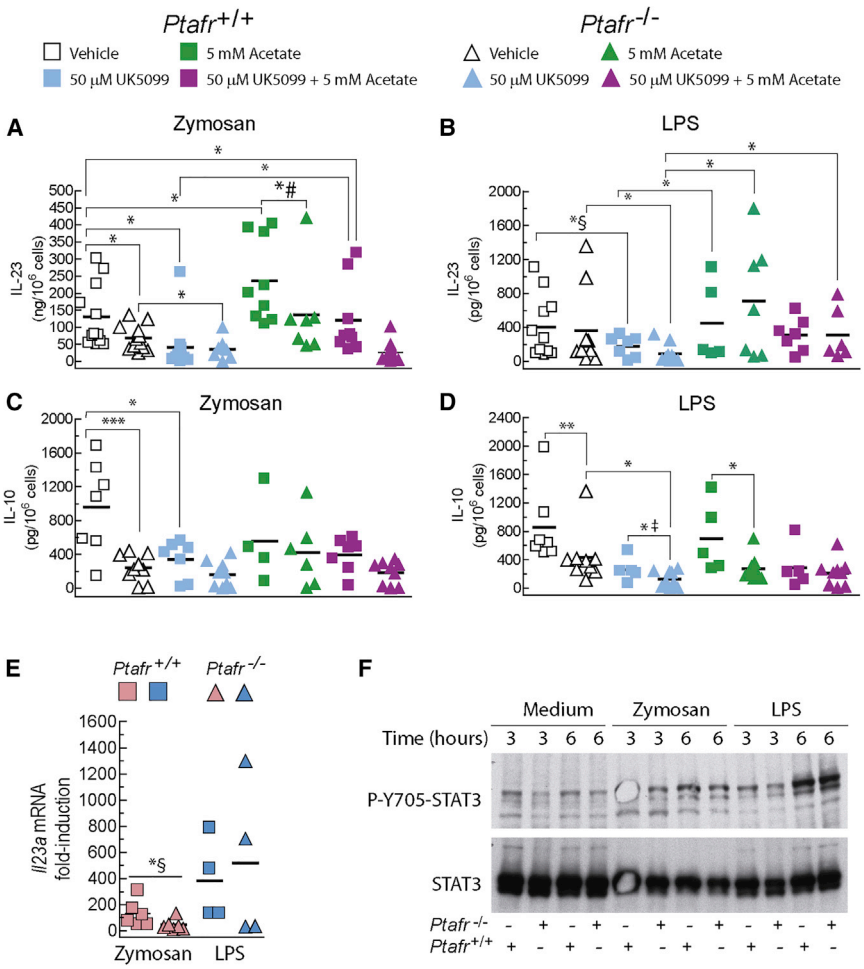

Figure 7. Effect of the Deletion of the *Ptafr* Gene on the Production of IL-23 and IL-10

BMDCs were cultured in medium supplemented with murine GM-CSF. On day 5, the floating cells were collected and plated before stimulation with 1 mg/mL zymosan and 10 μg/mL LPS.

(A and B) Effect of the preincubation with UK5099 and acetate on IL-23 protein production in BMDCs from WT and mice with deletion of *Ptafr* treated with zymosan (A) and LPS (B). Preincubation with the indicated additions was maintained for 1 h, and IL-23 was assayed at 24 h. Mean ± SEM. *$p < 0.05$, two-tailed Student's t test; #Mann-Whitney test; §Wilcoxon signed-rank test.

(C and D) Effect of UK5099 and acetate supplementation on the induction of IL-10 protein in BMDCs stimulated with zymosan (C) or LPS (D). Preincubation was maintained for 1 h, and protein was assayed at 24 h. Mean ± SEM. *$p < 0.05$, **$p < 0.01$, and ***$p < 0.001$, two-tailed Student's t test; ‡unpaired one-tailed Student's t test.

(E) Induction of *Il23a* mRNA in pools including BMDCs of three mice each stimulated with zymosan and LPS. Mean ± SEM. *$p < 0.05$, two-tailed Student's t test; §Wilcoxon signed-rank test.

(F) Effect of *Ptafr* deletion on Y705-STAT3 phosphorylation in BMDCs stimulated with 1 mg/mL zymosan and 10 μg/mL LPS. The experiment was carried out using a pool of BMDCs from three animals in each group. The granulocyte/macrophage colony-stimulating factor (GM-CSF) used for differentiation was washed from the media, and BMDCs were incubated in new medium for 3 h, prior to the addition of the stimuli. The times of 3 and 6 h after addition of the stimuli were selected for fixed-time experiments from the results of a previous study (Rodríguez et al., 2017).

See also Figure S5.

of zymosan energetic profile are the increases of the lactate/pyruvate ratio and of oxaloacetate. Reduction of oxaloacetate to malate by cytoplasmic malate dehydrogenase 1 and transport of malate into the mitochondria by the malate shuttle is a likely hypothesis in view of the steady levels of malate.

The ACLY inhibitor was active only in some instances. At first glance, this can be explained by the decrease of citrate and supports the notion that ACLY activity is not a universal requirement for acetylation (Wellen et al., 2009). Likewise, it has recently been reported that acetate can be formed from the decarboxylation of pyruvate by a nucleophilic attack by reactive oxygen species. Acetate is then converted into acetyl-CoA by ACSS2 and supports lipogenesis (Liu et al., 2018).

The biosynthesis of lipid mediators induced by zymosan depends on the mobilization of Ca^{2+} ions and the hydrolysis of phosphatidylcholines by $cPLA_2$, which parallels the metabolic rewiring of DCs (Figure S5). Through the *de novo* synthesis of AA, acetyl-CoA contributes to the generation of PGE_2, an autocrine mediator of IL-10 (Alvarez et al., 2009; MacKenzie et al., 2013) and IL-1β production (Zasłona et al., 2017). Acetyl-CoA is a substrate for the production of PAF by LPCAT2, and PAF is an autocrine activator of IL-23 production. These results suggest that in addition to the role of acetyl-CoA in the *trans*-activation of genes via acetylation of proteins, acetyl-CoA supports the biosynthesis of lipid mediators. This was confirmed in experiments using *Ptafr*$^{-/-}$ mice, which showed a lower production of IL-10 and IL-23 than WT mice. The stronger reduction in IL-10 than in IL-23 can be explained by the different mechanisms of transcriptional regulation of these cytokines. PGE_2 is a paracrine mediator of *IL23A* expression that induces the recruitment of CREB into an enhanceosome in which at least NF-κB and ATF2 are involved (Brain et al., 2013; Rodríguez et al., 2014). Unlike zymosan, LPS does not elicit an early activation of $cPLA_2$ and the ensuing release of AA and PAF biosynthesis (Figure S4F). Conversely, LPS enhances a delayed production of PGE_2 and PAF via induction of COX2 and LPCAT2 (Morimoto et al., 2010; Koga et al., 2013). This explains the distinct association of lipid mediators with each stimulus. CREB and STAT3 are the key transcription factors involved in *IL10 trans*-activation. Both factors can be activated by zymosan and LPS through different mechanisms. Zymosan recruits CREB to the *IL10* promoter via PGE_2 and cyclic AMP, while LPS activates STAT3 via TLR4 receptors and IFNβ. Although it has been suggested that PAF contributes to the activation of STAT3 (Koga et al., 2017), experiments did not confirm this mechanism.

These results disclose an autocrine mechanism for the production of cytokines that couples fatty acid-glycerophospholipid remodeling to energetic metabolism via acetyl-CoA, a critical substrate for histone acetylation and PAF biosynthesis. Given the involvement of lipid mediators and cytokines in inflammatory diseases, such as psoriatic arthritis, multiple sclerosis, and inflammatory bowel disease, these results suggest that the pharmacological modulation of the pyruvate-citrate-acetyl-CoA axis may provide cues to regulate cytokine production with molecules based on metabolic intermediates, following the path initiated by the therapeutic use of dimethyl fumarate in psoriatic arthritis and multiple sclerosis.

STAR★METHODS

Detailed methods are provided in the online version of this paper and include the following:

- KEY RESOURCES TABLE
- CONTACT FOR REAGENT AND RESOURCE SHARING
- EXPERIMENTAL MODEL AND SUBJECT DETAILS
  - Dendritic Cells
  - Mice
  - Ethics Statement
- METHOD DETAILS
  - Real-time RT-PCR
  - Western Blotting
  - Flow Cytometry
  - PKM2 Cross-Linking
  - Extracellular Lactate Assay
  - Extraction of Metabolites
  - Assay of Metabolites
  - Bioenergetic Analysis
  - Laser-Scanning Confocal Fluorescence Microscopy
  - Measure of Intracellular Ca^{2+} Transients
  - Chromatin Immunoprecipitation (ChIP) Assay
- QUANTIFICATION AND STATISTICAL ANALYSIS
- DATA AND SOFTWARE AVAILABILITY
  - Data Resources

SUPPLEMENTAL INFORMATION

Supplemental Information can be found online at https://doi.org/10.1016/j.celrep.2019.03.033.

ACKNOWLEDGMENTS

We thank Prof. Takao Shimizu of the University of Tokyo and Prof. Satoshi Ishii of Akita University for providing the *Ptafr*$^{-/-}$ mice. We thank Prof. Javier García-Sancho of Universidad de Valladolid for his help with the assay of Ca^{2+} transients. We thank Biobanco del Centro de Hemoterapia y Hemodonación de Castilla y León for providing buffy coats. C.M. is the recipient of a predoctoral grant from the Valladolid Section of Asociación Española contra el Cáncer (AECC). C.H.-S. is the recipient of a post-doctoral grant from Fundación de la Sociedad Española de Hematología y Hemoterapia. This work was supported by Plan Nacional de Salud y Farmacia under grants SAF2013-44521-R, SAF2017-83079-R, BFU2014-53469-P, and BFU2014-53469-P; Junta de Castilla y León/Fondo Social Europeo grant CSI035P17; and Fundación Domingo Martínez.

AUTHOR CONTRIBUTIONS

Conceptualization and Methodology, J.R.C.-R., O.M., N.F., and M.S.C.; Investigation, S.M., J.J.F., C.H.-S., S.A., T.A.S., O.M., and M.R.P.; Writing – Original Draft, J.R.C.-R. and M.S.C.; Writing – Review & Editing, J.R.C.-R., N.F., and M.S.C.; Resources and Supervision, J.R.C.-R., N.F., and M.S.C.

DECLARATION OF INTERESTS

J.R.C.-R. is a co-founder of and scientific adviser for Quentis Therapeutics, Inc.

Received: October 15, 2018
Revised: January 30, 2019
Accepted: March 8, 2019
Published: April 9, 2019

REFERENCES

Alvarez, Y., Municio, C., Alonso, S., Sánchez Crespo, M., and Fernández, N. (2009). The induction of IL-10 by zymosan in dendritic cells depends on CREB activation by the coactivators CREB-binding protein and TORC2 and autocrine PGE_2. J. Immunol. *183*, 1471–1479.

Anastasiou, D., Yu, Y., Israelsen, W.J., Jiang, J.K., Boxer, M.B., Hong, B.S., Tempel, W., Dimov, S., Shen, M., Jha, A., et al. (2012). Pyruvate kinase M2 activators promote tetramer formation and suppress tumorigenesis. Nat. Chem. Biol. *8*, 839–847.

Balmer, M.L., Ma, E.H., Bantug, G.R., Grählert, J., Pfister, S., Glatter, T., Jauch, A., Dimeloe, S., Slack, E., Dehio, P., et al. (2016). Memory $CD8^+$ T cells require increased concentrations of acetate induced by stress for optimal function. Immunity *44*, 1312–1324.

Basu, S.S., and Blair, I.A. (2011). SILEC: a protocol for generating and using isotopically labeled coenzyme A mass spectrometry standards. Nat. Protoc. *7*, 1–12.

Brain, O., Owens, B.M., Pichulik, T., Allan, P., Khatamzas, E., Leslie, A., Steevels, T., Sharma, S., Mayer, A., Catuneanu, A.M., et al. (2013). The intracellular sensor NOD2 induces microRNA-29 expression in human dendritic cells to limit IL-23 release. Immunity *39*, 521–536.

Brooks, G.A. (2018). The science and translation of lactate shuttle theory. Cell Metab. *27*, 757–785.

Bulusu, V., Tumanov, S., Michalopoulou, E., van den Broek, N.J., MacKay, G., Nixon, C., Dhayade, S., Schug, Z.T., Vande Voorde, J., Blyth, K., et al. (2017). Acetate recapturing by nuclear acetyl-CoA synthetase 2 prevents loss of histone acetylation during oxygen and serum limitation. Cell Rep. *18*, 647–658.

Comerford, S.A., Huang, Z., Du, X., Wang, Y., Cai, L., Witkiewicz, A.K., Walters, H., Tantawy, M.N., Fu, A., Manning, H.C., et al. (2014). Acetate dependence of tumors. Cell *159*, 1591–1602.

Domínguez-Andrés, J., Novakovic, B., Li, Y., Scicluna, B.P., Gresnigt, M.S., Arts, R.J.W., Oosting, M., Moorlag, S.J.C.F.M., Groh, L.A., Zwaag, J., et al. (2019). The itaconate pathway is a central regulatory node linking innate immune tolerance and trained immunity. Cell Metab. *29*, 211–220.e5.

Everts, B., Amiel, E., Huang, S.C.C., Smith, A.M., Chang, C.H., Lam, W.Y., Redmann, V., Freitas, T.C., Blagih, J., van der Windt, G.J., et al. (2014). TLR-driven early glycolytic reprogramming via the kinases TBK1-IKKε supports the anabolic demands of dendritic cell activation. Nat. Immunol. *15*, 323–332.

Gantner, B.N., Simmons, R.M., Canavera, S.J., Akira, S., and Underhill, D.M. (2003). Collaborative induction of inflammatory responses by dectin-1 and Toll-like receptor 2. J. Exp. Med. *197*, 1107–1117.

Gao, X., Wang, H., Yang, J.J., Liu, X., and Liu, Z.R. (2012). Pyruvate kinase M2 regulates gene transcription by acting as a protein kinase. Mol. Cell *45*, 598–609.

Hui, S., Ghergurovich, J.M., Morscher, R.J., Jang, C., Teng, X., Lu, W., Esparza, L.A., Reya, T., Le Zhan, Yanxiang Guo, J., et al. (2017). Glucose feeds the TCA cycle via circulating lactate. Nature *551*, 115–118.

Ishii, S., Nagase, T., Tashiro, F., Ikuta, K., Sato, S., Waga, I., Kume, K., Miyazaki, J., and Shimizu, T. (1997). Bronchial hyperreactivity, increased endotoxin lethality and melanocytic tumorigenesis in transgenic mice overexpressing PAF receptor. EMBO J. *16*, 133–142.

Ishii, S., Kuwaki, T., Nagase, T., Maki, K., Tashiro, F., Sunaga, S., Cao, W.H., Kume, K., Fukuchi, Y., Ikuta, K., et al. (1998). Impaired anaphylactic responses with intact sensitivity to endotoxin in mice lacking a PAF receptor. J. Exp. Med. *187*, 1779–1788.

Jha, A.K., Huang, S.C., Sergushichev, A., Lampropoulou, V., Ivanova, Y., Loginicheva, E., Chmielewski, K., Stewart, K.M., Ashall, J., Everts, B., et al. (2015). Network integration of parallel metabolic and transcriptional data reveals metabolic modules that regulate macrophage polarization. Immunity *42*, 419–430.

Koga, M.M., Bizzarro, B., Sá-Nunes, A., Rios, F.J., and Jancar, S. (2013). Activation of PAF-receptor induces regulatory dendritic cells through PGE_2 and IL-10. Prostaglandins Leukot. Essent. Fatty Acids *89*, 319–326.

Koga, M.M., Filgueiras, L.R., Jancar, S., and Rios, F. (2017). Platelet-activation factor receptor induces interleukin 10 production through STAT3 activation in dendritic cells. J. Immunobiol. *2*, 123.

Krawczyk, C.M., Holowka, T., Sun, J., Blagih, J., Amiel, E., DeBerardinis, R.J., Cross, J.R., Jung, E., Thompson, C.B., Jones, R.G., and Pearce, E.J. (2010). Toll-like receptor-induced changes in glycolytic metabolism regulate dendritic cell activation. Blood *115*, 4742–4749.

Kurczy, M.E., Forsberg, E.M., Thorgersen, M.P., Poole, F.L., 2nd, Benton, H.P., Ivanisevic, J., Tran, M.L., Wall, J.D., Elias, D.A., Adams, M.W., et al. (2016). Global isotope metabolomics reveals adaptive strategies for nitrogen assimilation. ACS Chem. Biol. *11*, 1677–1685.

Lampropoulou, V., Sergushichev, A., Bambouskova, M., Nair, S., Vincent, E.E., Loginicheva, E., Cervantes-Barragan, L., Ma, X., Huang, S.C., Griss, T., et al. (2016). Itaconate links inhibition of succinate dehydrogenase with macrophage metabolic remodeling and regulation of inflammation. Cell Metab. *24*, 158–166.

Li, X., Yu, W., Qian, X., Xia, Y., Zheng, Y., Lee, J.H., Li, W., Lyu, J., Rao, G., Zhang, X., et al. (2017). Nucleus-translocated ACSS2 promotes gene transcription for lysosomal biogenesis and autophagy. Mol. Cell *66*, 684–697.e9.

Liu, P.S., Wang, H., Li, X., Chao, T., Teav, T., Christen, S., Di Conza, G., Cheng, W.C., Chou, C.H., Vavakova, M., et al. (2017). α-ketoglutarate orchestrates macrophage activation through metabolic and epigenetic reprogramming. Nat. Immunol. *18*, 985–994.

Liu, X., Cooper, D.E., Cluntun, A.A., Warmoes, M.O., Zhao, S., Reid, M.A., Liu, J., Lund, P.J., Lopes, M., Garcia, B.A., et al. (2018). Acetate production from glucose and coupling to mitochondrial metabolism in mammals. Cell *175*, 502–513.e13.

MacKenzie, K.F., Clark, K., Naqvi, S., McGuire, V.A., Nöehren, G., Kristariyanto, Y., van den Bosch, M., Mudaliar, M., McCarthy, P.C., Pattison, M.J., et al. (2013). $PGE(_2)$ induces macrophage IL-10 production and a regulatory-like phenotype via a protein kinase A-SIK-CRTC3 pathway. J. Immunol. *190*, 565–577.

MacPherson, S., Horkoff, M., Gravel, C., Hoffmann, T., Zuber, J., and Lum, J.J. (2017). STAT3 Regulation of citrate synthase is essential during the initiation of lymphocyte cell growth. Cell Rep. *19*, 910–918.

Márquez, S., Fernández, J.J., Terán-Cabanillas, E., Herrero, C., Alonso, S., Azogil, A., Montero, O., Iwawaki, T., Cubillos-Ruiz, J.R., Fernández, N., and Crespo, M.S. (2017). Endoplasmic reticulum stress sensor IRE1α enhances IL-23 expression by human dendritic cells. Front. Immunol. *8*, 639.

Meiser, J., Krämer, L., Sapcariu, S.C., Battello, N., Ghelfi, J., D'Herouel, A.F., Skupin, A., and Hiller, K. (2016). Pro-inflammatory macrophages sustain pyruvate oxidation through pyruvate dehydrogenase for the synthesis of itaconate and to enable cytokine expression. J. Biol. Chem. *291*, 3932–3946.

Mews, P., Donahue, G., Drake, A.M., Luczak, V., Abel, T., and Berger, S.L. (2017). Acetyl-CoA synthetase regulates histone acetylation and hippocampal memory. Nature *546*, 381–386.

Michelucci, A., Cordes, T., Ghelfi, J., Pailot, A., Reiling, N., Goldmann, O., Binz, T., Wegner, A., Tallam, A., Rausell, A., et al. (2013). Immune-responsive gene 1 protein links metabolism to immunity by catalyzing itaconic acid production. Proc. Natl. Acad. Sci. U S A *110*, 7820–7825.

Mills, E.L., Ryan, D.G., Prag, H.A., Dikovskaya, D., Menon, D., Zaslona, Z., Jedrychowski, M.P., Costa, A.S.H., Higgins, M., Hams, E., et al. (2018). Itaconate is an anti-inflammatory metabolite that activates Nrf2 via alkylation of KEAP1. Nature *556*, 113–117.

Morimoto, R., Shindou, H., Oda, Y., and Shimizu, T. (2010). Phosphorylation of lysophosphatidylcholine acyltransferase 2 at Ser34 enhances platelet-activating factor production in endotoxin-stimulated macrophages. J. Biol. Chem. *285*, 29857–29862.

Morimoto, R., Shindou, H., Tarui, M., and Shimizu, T. (2014). Rapid production of platelet-activating factor is induced by protein kinase Cα-mediated phosphorylation of lysophosphatidylcholine acyltransferase 2 protein. J. Biol. Chem. *289*, 15566–15576.

Municio, C., Alvarez, Y., Montero, O., Hugo, E., Rodríguez, M., Domingo, E., Alonso, S., Fernández, N., and Crespo, M.S. (2013). The response of human macrophages to β-glucans depends on the inflammatory milieu. PLoS ONE *8*, e62016.

Palsson-McDermott, E.M., Curtis, A.M., Goel, G., Lauterbach, M.A., Sheedy, F.J., Gleeson, L.E., van den Bosch, M.W., Quinn, S.R., Domingo-Fernandez, R., Johnston, D.G., et al. (2015). Pyruvate kinase M2 regulates Hif-1α activity and IL-1β induction and is a critical determinant of the Warburg effect in LPS-activated macrophages. Cell Metab. *21*, 65–80.

Papathanassiu, A.E., Ko, J.-H., Imprialou, M., Bagnati, M., Srivastava, P.K., Vu, H.A., Cucchi, D., McAdoo, S.P., Ananieva, E.A., Mauro, C., and Behmoaras, J. (2017). BCAT1 controls metabolic reprogramming in activated human macrophages and is associated with inflammatory diseases. Nat. Commun. *8*, 16040.

Rodríguez, M., Domingo, E., Alonso, S., Frade, J.G., Eiros, J., Crespo, M.S., and Fernández, N. (2014). The unfolded protein response and the phosphorylations of activating transcription factor 2 in the trans-activation of *il23a* promoter produced by β-glucans. J. Biol. Chem. *289*, 22942–22957.

Rodríguez, M., Márquez, S., Montero, O., Alonso, S., García Frade, J., Sánchez Crespo, M., and Fernandez, N. (2016). Pharmacological inhibition of eicosanoids and PAF signaling impairs zymosan-induced release of IL-23 by dendritic cells. Biochem. Pharmacol. *102*, 78–96.

Rodríguez, M., Márquez, S., de la Rosa, J.V., Alonso, S., Castrillo, A., Sánchez Crespo, M., and Fernández, N. (2017). Fungal pattern receptors down-regulate the inflammatory response by a cross-inhibitory mechanism independent of interleukin-10 production. Immunology *150*, 184–198.

Rubic, T., Lametschwandtner, G., Jost, S., Hinteregger, S., Kund, J., Carballido-Perrig, N., Schwärzler, C., Junt, T., Voshol, H., Meingassner, J.G., et al. (2008). Triggering the succinate receptor GPR91 on dendritic cells enhances immunity. Nat. Immunol. *9*, 1261–1269.

Salem, N., Jr., Pawlosky, R., Wegher, B., and Hibbeln, J. (1999). *In vivo* conversion of linoleic acid to arachidonic acid in human adults. Prostaglandins Leukot. Essent. Fatty Acids *60*, 407–410.

Shirai, T., Nazarewicz, R.R., Wallis, B.B., Yanes, R.E., Watanabe, R., Hilhorst, M., Tian, L., Harrison, D.G., Giacomini, J.C., Assimes, T.L., et al. (2016). The glycolytic enzyme PKM2 bridges metabolic and inflammatory dysfunction in coronary artery disease. J. Exp. Med. *213*, 337–354.

Tannahill, G.M., Curtis, A.M., Adamik, J., Palsson-McDermott, E.M., McGettrick, A.F., Goel, G., Frezza, C., Bernard, N.J., Kelly, B., Foley, N.H., et al. (2013). Succinate is an inflammatory signal that induces IL-1β through HIF-1α. Nature *496*, 238–242.

Taylor, W.M., and Halperin, M.L. (1973). Regulation of pyruvate dehydrogenase in muscle. Inhibition by citrate. J. Biol. Chem. *248*, 6080–6083.

Uozumi, N., Kume, K., Nagase, T., Nakatani, N., Ishii, S., Tashiro, F., Komagata, Y., Maki, K., Ikuta, K., Ouchi, Y., et al. (1997). Role of cytosolic phospholipase A_2 in allergic response and parturition. Nature *390*, 618–622.

Vadas, P., Gold, M., Perelman, B., Liss, G.M., Lack, G., Blyth, T., Simons, F.E., Simons, K.J., Cass, D., and Yeung, J. (2008). Platelet-activating factor, PAF acetylhydrolase, and severe anaphylaxis. N. Engl. J. Med. *358*, 28–35.

Valera, I., Fernández, N., Trinidad, A.G., Alonso, S., Brown, G.D., Alonso, A., and Crespo, M.S. (2008). Costimulation of dectin-1 and DC-SIGN triggers the arachidonic acid cascade in human monocyte-derived dendritic cells. J. Immunol. *180*, 5727–5736.

Vats, D., Mukundan, L., Odegaard, J.I., Zhang, L., Smith, K.L., Morel, C.R., Wagner, R.A., Greaves, D.R., Murray, P.J., and Chawla, A. (2006). Oxidative metabolism and PGC-1beta attenuate macrophage-mediated inflammation. Cell Metab. *4*, 13–24.

Watanabe, R., Shirai, T., Namkoong, H., Zhang, H., Berry, G.J., Wallis, B.B., Schaefgen, B., Harrison, D.G., Tremmel, J.A., Giacomini, J.C., et al. (2017). Pyruvate controls the checkpoint inhibitor PD-L1 and suppresses T cell immunity. J. Clin. Invest. *127*, 2725–2738.

Wellen, K.E., Hatzivassiliou, G., Sachdeva, U.M., Bui, T.V., Cross, J.R., and Thompson, C.B. (2009). ATP-citrate lyase links cellular metabolism to histone acetylation. Science *324*, 1076–1080.

Zasłona, Z., Pålsson-McDermott, E.M., Menon, D., Haneklaus, M., Flis, E., Prendeville, H., Corcoran, S.E., Peters-Golden, M., and O'Neill, L.A.J. (2017). The induction of pro-IL-1β by lipopolysaccharide requires endogenous prostaglandin E_2 production. J. Immunol. *198*, 3558–3564.

STAR★METHODS

KEY RESOURCES TABLE

REAGENT or RESOURCE	SOURCE	IDENTIFIER
Antibodies		
Mouse Anti-pyruvate dehydrogenase E1-α subunit	Abcam	ab110334; RRID: AB_10866116
Rabbit Anti-P-S293-pyruvate dehydrogenase E1-α subunit	Abcam	ab92696; RRID: AB_10711672
Mouse Anti-DC-SIGN	R&D Systems	MAB 161; RRID: AB_357808
Rabbit Anti-ACSS2	Cell Signaling	#3658; RRID: AB_2222710
Mouse Anti-β-tubulin	Sigma	T8328; RRID: AB_1844090
Mouse Anti-β-actin	Sigma	A 1978; RRID: AB_476692
Anti-TATA-box binding protein	Diagenode	C15200002
Rabbit-Anti-histone H3	Abcam	ab1791; RRID: AB_302613
Rabbit-Acetyl-K9-histone H3	Millipore	#4-1003; RRID: AB_1977254
Rabbit-P-S10-histone H3	Millipore	#04-817; RRID: AB_1163440
Rabbit Anti-PKM2	Cell Signaling	#3198S; RRID:AB_2269803
Rabbit Anti-STAT3	Cell Signaling	#9132; RRID: *AB_ 2491009*
Rabbit Anti-Phospho-STAT3 (Tyr705)	Cell Signaling	#9131; RRID: AB_331587
Rabbit Anti-SUCNR1/GPR91	Novus Biologicals	NBP2-24549
Biological Samples		
Human monocyte-derived dendritic cells	Biobanco del Centro de Hemoterapia y Hemodonación de Castilla y León	http://www.centrodehemoterapiacyl.es/
Chemicals, Peptides, and Recombinant Proteins		
Zymosan	Sigma-Aldrich	Cat#Z4250 CAS: 58856-93-2
LPS	Sigma-Aldrich	Cat# L2630
Dichloroacetate	Sigma-Aldrich	Cat#347795 CAS: 2156-56-1
Acetate	Sigma-Aldrich	Cat#71196 CAS:127-09-3
Succinate	Sigma-Aldrich	Cat#S3674 CAS: 110-15-6
Rotenone	Sigma-Aldrich	Cat#R8875 CAS: 83-79-4
UK5099	Sigma-Aldrich	Cat#PZ0160; CAS 56396-35-1
L-Glutamine	GIBCO	Cat#A2916801
Recombinant human GM-CSF premium grade	Miltenyi Biotec	130-093-868; CAS: 83869-56-1
Recombinant murine GM-CSF	Peprotech	# 315-03; CAS: 83869-56-1
Recombinant human IL-4	R&D Systems	204-IL
N-(2,3-di-2-thienyl-6-quinoxalinyl)-N'-(2-methoxyethyl)urea (ACSS2i)	ChemBridge Corp., San Diego, CA.	ID# 7032008; CAS: 508186-14-9
ML-265/TEPP-46	Cayman	Ref: 13942; CAS: 1221186-53-3
Acetonitrile	Merck Millipore	Ref: 1000291000 CAS: 75-05-08
CB-839	Selleckchem	Catalog No.S7655; CAS: 1439399-58-2
BMS 303141	Tocris	Catalog No. 4609; CAS: 943962-47-8
Cell-Tak®	Corning	Cat#354240
Disuccinimidyl suberate	Thermo Fisher Scientific.	Cat#21655; CAS: 68528-80-3
Mouse IL-23 ELISA kit	Thermo Fisher Scientific	BMS6017
Mouse IL-10 ELISA kit	Thermo Fisher Scientific	EM2IL10
TRIzol	Thermo Fisher Scientific	Cat#15596026
Hoechst 33342, trihydrochloride, trihydrate	Thermo Fisher Scientific	Ref: H1399
Critical Commercial Assays		
Nuclear extract kit	Active Motif	Catalog number: 40010
Seahorse XF Cell Mito Stress Test Kit	Agilent	Ref: 103010-100

(*Continued on next page*)

Continued		
REAGENT or RESOURCE	SOURCE	IDENTIFIER
Lactate assay kit II	Sigma-Aldrich	Ref: MAK065
Deposited Data		
Raw data	Mendeley Data	https://doi.org/10.17632/56x8ypv8g4.1
Experimental Models: Cell Lines		
Monocyte-derived dendritic cells from healthy donors	Biobanco del Centro de Hemoterapia y Hemodonación de Castilla y León	http://www.centrodehemoterapiacyl.es/
Experimental Models: Organisms/Strains		
C57BL/6 mice *Ptfar*−/− and *Ptfar*+/+	Department of Lipid Signaling, National Center for Global Health and Medicine, Tokyo, Japan	http://mus.brc.riken.jp/
Oligonucleotides		
See Table S1 for oligo information		N/A
Software and Algorithms		
GraphPad Prism 4	GraphPad Software	https://www.graphpad.com/
MS^E Technology	Waters	http://www.waters.com/
Kaluza software version 1.1	Beckman Coulter Life Sciences	http://www.beckmancoulter.com/
Leica LAS AF Lite	Leica	http://www.leicabiosystems.com/
Simple PCI 6.6 Hamamatsu software	Hamamatsu Photonics	http://www.hamamatsu.com
Adobe Photoshop CS5.1	Adobe Systems	https://www.adobe.com/
Other		
StrataTM C-18E SPE cartridges	Phenomenex®	Ref: 8B-S001-HCH
Amicon MWCO 10 kDa centrifugal filters	Sigma	Ref: Z677108-96EA
Acquity CORTECS UPLC® C18	Waters	Product Number: 176003149
Luna® Omega Polar C18 Columns	Phenomenex®	Part number: 00D-4748-AN
Bioruptor™	Diagenode	Catalog # UCB-200
Gallios Flow Cytometer	Beckman Coulter Life Sciences	https://www.beckman.es/coulter-flow-cytometers/gallios

CONTACT FOR REAGENT AND RESOURCE SHARING

Further information and requests for resources and reagents should be directed to and will be fulfilled by the Lead Contact, Mariano Sánchez Crespo (mscres@ibgm.uva.es).

EXPERIMENTAL MODEL AND SUBJECT DETAILS

Dendritic Cells

DCs were obtained from human mononuclear cells collected from buffy coats of healthy donors provided by Centro de Hemoterapia de Castilla y León. The differentiation of monocytes was carried out in the presence of 800 U/ml GM-CSF and 500 U/ml IL-4 for 5 days and assessed by immunofluorescence flow cytometry of CD40, CD80, CD83, CD86, CD32, CD11b, CD11c, dectin-1, and DC209 as reported (Valera et al., 2008; Municio et al., 2013). Culture was carried out in RPMI 1640 medium containing 11.1 mM D-glucose and 4 mM glutamine. 10% FBS was maintained during the differentiation process and reduced to 2% prior to the initiation of the experiments. These conditions were used to replicate the experimental setting of Seahorse assays.

Mice

Ptafr$^{-/-}$ mice were a generous gift from Prof. Takao Shimizu (Department of Lipid Signaling, National Center for Global Health and Medicine, University of Tokyo, Japan) and Prof. Satoshi Ishii (Dpt. of Immunology, Akita University, Japan). Bone marrow from the femora and tibiae from three month old, male mice were used to obtain BMDCs from wild WT C57BL/6 and *Ptafr*$^{-/-}$ mice by culture in the presence of 10 ng/ml murine GM-CSF for 5 days.

Ethics Statement

The study was approved by the Bioethical Committee of the Spanish Council of Research (CSIC) and the written informed consent of all healthy donors was obtained at Centro de Hemoterapia y Hemodonación de Castilla y León Biobank. The participants received

written consent according to the regulations of the Biobank and the researchers received the samples in an anonymous way. The process is documented by the Biobank authority according to the specific Spanish regulations. The animal experiments were carried out with permission of the local authority and conform to institutional standards. The ethics committee approved this procedure before starting the study.

METHOD DETAILS

Real-time RT-PCR

Total RNA was obtained by TRIzol/chloroform extraction and used for RT reactions. Cycling conditions were adapted to each set of primers. *GAPDH* was used as a housekeeping gene to assess the relative abundance of the different mRNA using the comparative cycle threshold method. The procedure was used to assay *IL10*, *IL23A*, *TNF*, *IL1B*, *ACSS2*, *PDL1*, and *ACLY* mRNA. Primer sequences are shown in Table S1.

Western Blotting

Proteins were separated by electrophoresis in SDS/PAGE and transferred to nitrocellulose membranes. The membranes were used for the immunodetection of P-Y705-STAT3, STAT3, PKM2, histone H3, pyruvate dehydrogenase E1-α subunit, P-S293-pyruvate dehydrogenase E1-α subunit, acetyl-K9-histone H3, and P-S10-histone H3. For immunoblots directed to assay nuclear proteins, the nuclear extracts were obtained using a nuclear extract kit. Anti-TATA-box binding protein (TBP), anti-histone H3 and anti-β-tubulin Abs were used for protein load control.

Flow Cytometry

The expression of GPR91, CD14, and CD1a was assayed by indirect immunofluorescence using a labeled secondary Ab, before washing and formaldehyde fixation steps. Isotype-matched irrelevant Abs were used as control. At least 10,000 cells were analyzed per sample. Kaluza software version 1.1 was used for quantitative data analysis.

PKM2 Cross-Linking

DCs were treated with 50 μM ML-265 or DMSO for 30 min and at the end of this period, stimulated for 1 hour with zymosan or LPS. DCs were washed three times with PBS at pH 8 and crosslinking was carried out with 650 μM disuccinimidyl suberate for 30 minutes at room temperature as reported by Palsson-McDermott et al., (2015). The reaction was quenched by addition of Tris-HCl, pH 7.5, to 100 mM final. Lysates were analyzed by 8% SDS-PAGE and Western Blot.

Extracellular Lactate Assay

Lactate was assayed using a colorimetric test in cell supernatants deproteinized by filtration with 10 kDa MWCO spin. The soluble fraction was assayed using a Lactate Assay Kit II.

Extraction of Metabolites

DCs were treated with cold acetonitrile:methanol:water (2:2:1, v/v/v), frozen in cold nitrogen, and thawed prior to bath sonication for 15 min at 4°C. After an additional cycle of freezing and sonication, the extracting mixture was kept at −20°C for 1 h, and then centrifuged at 15000 x g at 4°C for 15 min for deproteinization. The supernatant was recovered and evaporated to dryness (Kurczy et al., 2016). The solid residue was solubilized in acetonitrile:water (1:1, v/v). For UPLC-MS analysis, the sample solvent was evaporated to dryness and the pellet resuspended in Milli-Q (MQ) water.

Assay of Metabolites

The assay of intracellular pyruvate, lactate, oxaloacetate (measured as the adduct $[M\text{-}H_2O+H]^+$), citrate, α-ketoglutarate, succinate, itaconate, and malate was carried out using an UPLC-MS assay. The chromatographic separation was carried out with an Acquity CORTECS UPLC® C18 column directly interfaced into the electrospray ionization source of a Q-TOF mass spectrometer (SYNAPT HDMS G2, Waters). An elution gradient involving the eluents (A) H_2O:methanol:formic acid (95:5:0.1, v/v/v) with 5 mM ammonium formate, and (B) 100% acetonitrile with 0.1% formic acid and 5 mM ammonium formate, was run from 95% A to 20% A in 4 min, then isocratic until 4.5 min, to come again to 95% A at 6 min and kept to 95% A for an additional period of 2 min (8 min elution period), at a flow rate of 0.2 mL/min. MS analysis was performed in the negative ion mode using a MS^E method that allows simultaneous detection of analytes through a low energy function (full scan) and a high energy function (collision energy) with ion partial fragmentation. For the assay of AA metabolites, the supernatants were extracted into ethanol (15% final concentration), applied into StrataTM C-18E SPE cartridges, eluted into methanol, and evaporated to dryness under N_2, before the chromatographic separation in the aforementioned system. The chromatographic separation of short-chain acyl-CoA was carried out in a Luna® Omega Polar C18. The chromatography was carried out using eluent (A) MQ water with 15 mM ammonium acetate, and (B) methanol:acetonitrile (2:8, v/v) with 8.3 mM ammonium acetate. The gradient consists of 97% A to 5% over an 8-min period, to come back to 97% A over 1 min and kept so for 1 min (10 min of total elution run), at a flow rate of 0.5 mL/min. The analytes were detected in the positive ion mode. Acetyl-CoA was identified by monitoring the m/z 303.1375 amu (atomic mass units) fragment in the high-energy function

that results after the specific neutral loss of 507 amu from the *m/z* 810.1346 amu $[M+H]^+$ ion of the acetyl-CoA (Basu and Blair, 2011) (Figure S6).

Bioenergetic Analysis

Bioenergetic analyses were carried out in a Seahorse Bioscience XFe96 Extracellular Flux Analyzer. 10^5 DCs were adhered with Cell-Tak® to Seahorse plates and stimulated with zymosan and LPS after a stabilization period. OCR and ECAR were analyzed according to the XF Cell Mito Stress Test kit protocol in XF media under the experimental conditions and in response to oligomycin, FCCP, and rotenone plus antimycin A. Normalization was conducted by absorbance using Hoechst 33342 assay.

Laser-Scanning Confocal Fluorescence Microscopy

DCs were seeded on poly-lysine-coated glass coverslips for 12 hours and then stimulated with zymosan particles. Cells were fixed with 10% formaldehyde in PBS and stained with anti-SUCNR1 and anti-DC-SIGN Ab, and goat anti-rabbit IgG Ab labeled with Alexa Fluor®488 or Alexa Fluor®594. The coverslips were examined by laser-scanning confocal fluorescence microscopy using a Leica TCS SP5 apparatus equipped with a white-light laser and a Leica 63PL APO NA 1.40 oil immersion objective. Image analysis and subcellular colocalization fluorograms were generated and analyzed using a Leica confocal software package and Adobe Photoshop CS5.1 software.

Measure of Intracellular Ca^{2+} Transients

DCs seeded on poly-ornithine coated glasses were loaded with 4 μM fura 2-acetoxymethyl ester for 1 h at room temperature in a medium containing: 145 mM NaCl, 5 mM KCl, 1 mM $CaCl_2$, 1 mM $MgCl_2$, 10 mM glucose, and 10 mM HEPES sodium, pH 7.4. DCs were then washed with fresh medium and the cell-containing coverslips were mounted under the microscope (Nikon Diaphot). Test solutions were applied by continuous perfusion at 2 ml/min. For fluorescence measurements, DCs were alternately epi-illuminated at 340 and 380 nm, and light emitted above 520 nm was recorded using a Hamamatsu Digital Camera C4742-98 handled by Simple PCI 6.6 Hamamatsu software. Consecutive frames obtained at 340 and 380 nm excitation were ratioed pixel by pixel using ImageJ software.

Chromatin Immunoprecipitation (ChIP) Assay

ChIP assays were conducted with Ab against acetyl-K9-histone H3. DCs were fixed with 1% formaldehyde and cross-linking was finished by 0.125 M glycine. Chromatin sonication was carried out using a Bioruptor™ device. The chromatin solution was precleared by adding Protein A/G PLUS-Agarose. After preclearing, anti-acetyl-K9-histone H3 Ab or irrelevant Ab were added for overnight incubation at 4°C, and then Protein A/G PLUS-Agarose was added and incubated for an additional period of 2 hours at 4°C. Cross-links were reversed by heating and the DNA bound to the beads isolated by extraction with phenol/chloroform/isoamylalcohol. Irrelevant Ab and sequences of the *IL12A* promoter were used as control of binding specificity. Results are expressed as percentage of input. Primer sequences are shown in Table S1.

QUANTIFICATION AND STATISTICAL ANALYSIS

Data are represented as the mean ± SEM and were analyzed with the Prism 4.0 statistical program. Repeated-measures one-way and two-way ANOVA analyses were performed. When data did not follow normal distribution nor had equal variances, log-transformation was applied previous to analysis. Comparison between experimental groups was carried out using unpaired or paired two-tailed Student's t test, Wilcoxon signed-rank test, and Mann-Whitney. Kruskal-Wallis test and Friedman tests were used for multiple comparison in the case of non-normally distributed samples. Statistical details are shown in the figure legends. Differences were considered significant for $p < 0.05$.

DATA AND SOFTWARE AVAILABILITY

Data Resources

The raw data have been uploaded to Mendeley Data under the accession number https://doi.org/10.17632/56x8ypv8g4.1